



Investigation of reorganization of a nanocrystalline grain boundary network during biaxial creep deformation of nanocrystalline Ni using molecular dynamics simulation

Snehanshu Pal¹ · Md. Meraj^{1,2}

Received: 6 May 2019 / Accepted: 20 August 2019 / Published online: 29 August 2019
© Springer-Verlag GmbH Germany, part of Springer Nature 2019

Abstract

In this paper, simulated biaxial creep deformation behaviour for nanocrystalline (NC) nickel (Ni) has been performed at various applied load (i.e. 1 GPa, 1.4 GPa, 2 GPa, 2.5 GPa and 3 GPa) for a particular temperature (i.e. 1210 K) using molecular dynamics (MD) simulation to investigate underlying deformation mechanism based on the structural evolution during biaxial creep process. Primary, secondary and tertiary stages of creep are observed to be exhibited significantly only at 3 GPa applied stress. While, only primary and secondary stages of creep are exhibited at 1 GPa applied stress. Atomic structural evaluation, dislocation density, shear strains, atomic trajectory, inverse pole figures and grain orientation with texture distribution have been carried out to evaluate structural evolution. Stress exponent (m) for NC Ni is analysed for a particular creep temperature (i.e. 1210 K) and obtained m value is 1.30. According to shear strains counter plot, accumulation of higher shear strains are observed at grain boundary (GB) during biaxial creep deformation. It is found that dislocation density during biaxial creep is increased with the progress of creep process. Grain rotation and texture evaluation during biaxial creep process are studied using grain tracking algorithm (GTA). Grain rotation in ultrafine-grained NC Ni specimen during biaxial creep deformation is happened and exhibits almost distinct distribution, which is occurred due to the atomic shuffling within the GBs. Grain growth of ultrafine grained NC Ni is observed during biaxial creep deformation which is caused by mechanical stress.

Keywords Biaxial creep · Molecular dynamics · Nanocrystalline · Diffusion control creep · Nickel

Introduction

Nanocrystalline (NC) metals grab significant attention of both material scientists and engineers due to their high mechanical strength and unique deformation nature with respect to their coarse-grained polycrystalline counterparts and accordingly they become a comparatively better choice for structural application [1–7]. However, in order to enhance their applicability as structural materials, it is necessary to improve their creep resistance property. In this perspective, thorough understanding of high-temperature deformation mechanism of NC metals

at the atomic scale is highly crucial for achieving improved creep properties and several relevant majorly experimental based investigations have been started over the last few decades [8–14].

In addition to uniaxial creep studies, several investigations on biaxial creep behaviour by experimentations for coarse-grained metals have been performed [15–28]. It is reported that the dislocation creep mechanism is the major cause for deformation at different stress conditions [19, 20]. Tung et al. have also studied the biaxial creep for coarse grained materials by experimentally and it is found that dislocations, as well as grain boundary sliding with diffusional accommodation creep mechanisms, are active during biaxial creep deformation [18].

In case of ultrafine nanocrystalline metal having grain size in the order of 10 nm, conventional intra-granular dislocation governed deformation mechanisms become subdued [29, 30]. Plastic deformation of such ultrafine grained NC metal is controlled by grain boundary sliding [31–33], grain rotation [34–36], and grain boundary migration [37–39]. Simultaneously activated multiple mechanisms, such as grain

✉ Snehanshu Pal
snehanshu.pal@gmail.com; pals@nitrrkl.ac.in

¹ Department of Metallurgical and Materials Engineering, National Institute of Technology Rourkela, Rourkela 769008, India

² Department of Mechanical Engineering, G H Raisoni Academy of Engineering & Technology, Nagpur 440016, India

rotation and grain boundary migration, can be operative and responsible for the plasticity NC metal [40]. All the mechanisms of plastic deformation of NC metal basically represent movement of groups of atoms collectively, which in turn change the internal grain architecture [41]. Rotation of two adjacent grains causes variation in orientation angle between the grains and features of grain boundary present between them. In this perspective, molecular dynamics (MD) simulation is found to be effective to get insight of operative deformation mechanisms for ultrafine grained NC metal. Hasnaoui et al. [42] have performed MD simulation and revealed that the appearance of shear planes in nanocrystalline Ni due to the arrangement of GB planes by dint of grain rotation, grain boundary sliding and grain boundary migration and that phenomenon causes localized shear deformation along with grain coalescence and growth. In this line, Rupert [43] has also reported that grain boundary network connectivity is highly responsible for strain localization. At this juncture, it is understood that grain boundary network connectivity, grain boundary sliding and grain boundary migration may play an important role for creep deformation of NC metals and accordingly the study of the evolution of grain rotation and the internal grain architecture during creep deformation process is highly essential. Through experimentation, very limited information has been extracted on atomic-scale structure evolution during creep deformation of NC metals as it is known that atomic-level experimental techniques along with in-situ characterization techniques are very difficult to implement for capturing the dynamics of deformation [29, 44–50]. Recent trends of research in this area reveals that molecular dynamics (MD) simulation based study of atomic-scale mechanisms responsible for creep deformation of ultrafine NC metals having grain size (diameter, d) in the order of 10 nm, is reliable [7, 51–61]. Numerous researchers have done creep study for NC metals by MD simulations previously and it is reported that grain boundary (GB) diffusional (Coble creep) creep mechanism is the operative and major factor for deformation of ultrafine grained NC metals under low and medium level of stress [7, 51–55, 61–65]. The uniaxial tensile creep behaviour study for ultrafine-grained NC Ni metal using MD simulation has been performed previously and Coble creep is found to be dominant creep mechanism for NC Ni having less than 10 nm grain size [7, 54].

The investigation of biaxial creep for ultrafine-grained NC metals (grain size in the order ~ 10 nm) is essential, but the study of biaxial creep deformation behaviour and internal grain structure evolution dynamics during creep deformation for such ultrafine grained NC metals is not reported until date in the literature as per author knowledge. Therefore, we have performed MD simulation-based investigation of biaxial creep deformation behaviour of NC Ni. The objective of the current study is to investigate the effect of the biaxial state of stress on the creep behaviour NC Ni (having grain size ~ 6 nm) and

provide rational insight of the underlying biaxial creep deformation mechanism at the atomic scale. In order to do so, grain rotation and evolution of internal grain structure of NC specimen during biaxial creep deformation have been investigated. Diffusional creep mechanism is dominated during uniaxial creep deformation process [7], while dislocations, as well as grain boundary diffusion, creep mechanisms are operative during biaxial creep deformation for same grain size NC Ni specimen. Thus, the deformation mechanism is different for biaxial as compared with uniaxial creep deformation on nanocrystalline metal. It is well known that the state of stress has a huge influence on deformation behaviour of metals so only understanding of uniaxial creep behaviour will not be sufficient. Therefore, biaxial creep deformation simulation is necessary to perform. The motivation of the work is to understand the influence of stress state on creep properties of NC metals and its associated underlying mechanistic rationality, because such knowledge will help as well as create interest to find out the ways to achieve better creep resistance under biaxial stress condition.

Molecular dynamics simulation details

A nanocrystalline (NC) cubic Ni specimen with an average grain size ~ 6 nm is generated by Voronoi construction algorithm [66] under full three-dimensional periodic boundary conditions. The full specimen of NC Ni contains 14 uniform grains with random position and crystallographic orientations. The dimension of cubic NC Ni specimen is taken as $14.08 \text{ nm} \times 14.08 \text{ nm} \times 14.08 \text{ nm}$ for performing MD simulation and the cubic simulation box contains 240,678 atoms. Before initiating the biaxial creep process, energy minimization of NC Ni specimen is carried out using the conjugate gradient algorithm with 2 fs time step. Then, the NC Ni specimen is equilibrated at 1210 K ($\sim 0.72 \cdot T_m$) temperature for 30 ps using *NVT* ensemble to control temperature by Nose-Hoover thermostat method [67, 68]. Calculated melting temperature (T_m) of NC Ni having average grain size 6 nm is ~ 1674 K and the same is represented in Fig. 1. After that, NC Ni specimen is allowed to deform along the X- and Y-direction under constant biaxial applied load/stress state in the form of pressure using the Berendsen barostat method [69] and no stress is applied in Z-directions. The equivalent biaxial creep strain is calculated using the following formula.

Calculated strain for X-direction is given below,

$$\varepsilon_x = \frac{l_x - l_{0x}}{l_{0x}} \quad (1)$$

where l_x and l_{0x} are the instantaneous length of the specimen along X-direction under applied stress and initial length of the specimen along X-direction respectively.

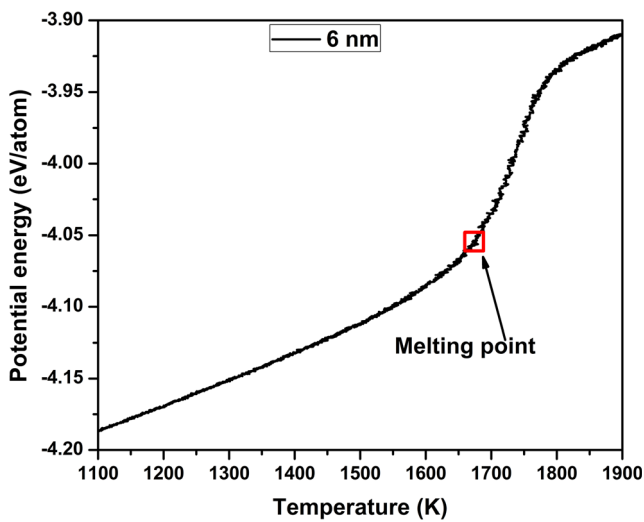


Fig. 1 Plot of potential energy vs. temperature to determine the melting point for NC Ni having average grain size 6 nm specimen

Calculated strain for Y-direction is given below,

$$\epsilon_y = \frac{l_y - l_{0y}}{l_{0y}} \tag{2}$$

where l_y and l_{0y} are the instantaneous length of the specimen along Y-direction under applied stress and initial length of the specimen along Y-direction respectively.

Effective strain (ϵ_{eff}) formula from von Mises criterion is given below.

For von Mises criterion, the effective strain is

$$\epsilon_{eff} = \frac{\sqrt{2}}{3} \left\{ (\epsilon_x - \epsilon_y)^2 + (\epsilon_y - \epsilon_z)^2 + (\epsilon_z - \epsilon_x)^2 \right\}^{1/2} \tag{3}$$

where ϵ_x , ϵ_y , and ϵ_z are the strain in the X-, Y-, and Z-direction respectively.

If $\epsilon_z = 0$, then the modified formula from Eq. (3) for equivalent biaxial creep strain calculation is given below

$$\epsilon_{eff} = \frac{\sqrt{2}}{3} \left\{ (\epsilon_x - \epsilon_y)^2 + (\epsilon_y - 0)^2 + (0 - \epsilon_x)^2 \right\}^{1/2} \tag{4}$$

$$\epsilon_{eff} = \frac{\sqrt{2}}{3} \left\{ (\epsilon_x - \epsilon_y)^2 + (\epsilon_y)^2 + (-\epsilon_x)^2 \right\}^{1/2} \tag{5}$$

$$\epsilon_{eff} = \frac{\sqrt{2}}{3} \left\{ (\epsilon_x)^2 + (\epsilon_y)^2 - 2\epsilon_x\epsilon_y + (\epsilon_y)^2 + (\epsilon_x)^2 \right\}^{1/2} \tag{6}$$

$$\epsilon_{eff} = \frac{\sqrt{2}}{3} \left\{ 2(\epsilon_x)^2 + 2(\epsilon_y)^2 - 2\epsilon_x\epsilon_y \right\}^{1/2} \tag{7}$$

$$\epsilon_{eff} = \frac{(\sqrt{2})^2}{3} \left\{ \epsilon_x^2 + \epsilon_y^2 - \epsilon_x\epsilon_y \right\}^{1/2} \tag{8}$$

$$\epsilon_{equi} = \frac{2}{3} \left(\epsilon_x^2 + \epsilon_y^2 - \epsilon_x\epsilon_y \right)^{1/2} \tag{9}$$

where ϵ_{equi} is the equivalent strain for bi-axial creep, ϵ_x is the strain in the X-direction and ϵ_y is the strain in Y-direction. According to von Mises criterion, the effective stress (σ_{eff}) is

$$\sigma_{eff} = \frac{1}{\sqrt{2}} \left\{ [(\sigma_x - \sigma_y)^2 + (\sigma_y - \sigma_z)^2 + (\sigma_z - \sigma_x)^2] \right\}^{1/2} \tag{10}$$

where σ_x , σ_y , and σ_z are the stress in the X-, Y-, and Z-direction respectively.

If $\sigma_z = 0$, and $\sigma_x = \sigma_y$ then the modified formula from Eq. (10) for the effective stress for equivalent biaxial creep is given below

$$\sigma_{eff} = \frac{1}{\sqrt{2}} \left\{ [(\sigma_x - \sigma_x)^2 + (\sigma_x - 0)^2 + (0 - \sigma_x)^2] \right\}^{1/2} \tag{11}$$

$$\sigma_{eff} = \frac{1}{\sqrt{2}} \left\{ [(0)^2 + (\sigma_x)^2 + (-\sigma_x)^2] \right\}^{1/2} \tag{12}$$

$$\sigma_{eff} = \frac{1}{\sqrt{2}} \left\{ 2(\sigma_x)^2 \right\}^{1/2} \tag{13}$$

$$\sigma_{eff} = \sigma_x \tag{14}$$

Thus, it is cleared from Eq. (14) that no any effective value of stress.

Simulated biaxial creep curves are performed under different constant biaxial stress state such as 1, 1.4, 2, 2.5, and 3 GPa at 1210 K temperature. Now, equivalent biaxial creep rate and minimum creep rate curves are calculated from the simulated biaxial creep curves. Time step of 2 fs is taken and periodic boundary conditions (PBCs) are applied in three directions for performing all the biaxial creep simulations, and melting point calculation. PBCs are a set of boundary conditions which are often chosen for approximating a large (infinite) size system by using a finite size system. Hence, specimen consists of 14 randomly oriented grains is fine to some extent for predicting the macroscopic features like the Taylor factor for materials by using PBCs in all three directions. All the atomistic calculations such as biaxial creep and melting point are executed using LAMMPS [70] with EAM FS (embedded atom model Finnis-Sinclair) potential developed by Mendeleev et al. [71] which is applicable for Ni systems. Atomic configuration snapshots capturing, atomic trajectory, CSP analysis, atomic strain, and dislocation extraction have performed using OVITO [72]. Grain tracking algorithm (GTA) is the post-processing technique, which is used to convert the positions of the atoms in the simulation cell into the structural measurements [41, 73] during biaxial creep process. The measured crystallographic orientation of all grains as well as the overall specimen texture are analysed in nanocrystalline materials such as inverse pole figures, grain rotation and orientation maps via GTA [41, 73].

Results and discussions

Discussion on simulated biaxial creep curve and corresponding creep rate

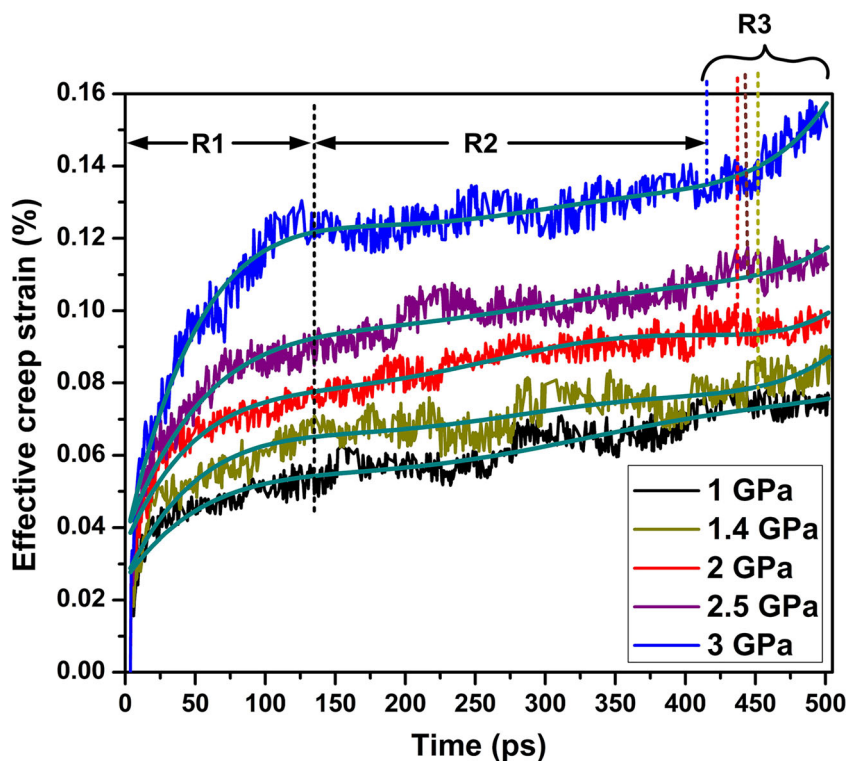
Effective creep strain vs. time curves for various applied biaxial stresses (i.e. 1, 1.4, 2, 2.5, and 3 GPa) are presented in Fig. 2 to study the effect of applied biaxial stress on the biaxial creep behaviour at 1210 K creep temperature. The biaxial creep curves (refer Fig. 2) constitute a short primary stage of creep (denoted as R1) followed by a longer secondary stage of creep (denoted as R2) and subsequently very short tertiary stage of creep (denoted as R3). At the initial stage of creep curve, a sharp rise in effective creep curve is observed for all the three cases studied here. This kind of sharp rise in effective creep strain is known as primary creep and creep rate is observed to be decreased in this stage with increasing creep time. Duration and rise in effective strain in primary creep stage is increased with the increasing applied biaxial stress. Then the secondary stage of creep initiates, which prevalent for a comparatively longer period and exhibit almost constant creep rate. It is observed from Fig. 2 that secondary stage of creep is decreased with increasing applied biaxial stress. Just after secondary stage of creep, tertiary stage of creep is observed only when the ultrafine-grained NC Ni specimen is subjected to higher biaxial load. Tertiary stage of creep is observed to be increased with increasing applied biaxial stress. In case of creep deformation occurring under 1 GPa applied biaxial

stress, tertiary creep regime is absent up until 500 ps time period (refer Fig. 2). As the applied biaxial stress on ultrafine-grained NC Ni specimen increases, the effective creep strain curves are shifted upward for 1210 K creep temperature (refer Fig. 2). Similar trend of shifting of creep curves for biaxial creep phenomena have also been observed previously through experimentations for coarse-grained metals [18, 20, 23]. Calculated effective creep rate-time curves for NC Ni at different biaxial applied stresses (i.e. 1, 1.4, 2, 2.5 and 3 GPa) are represented in Fig. 3. Biaxial creep strain rate in the primary stage of creep (R1) is decreased with increasing the creep time. It is observed that the effective creep rate in the primary stage of creep is shifted towards upward with increasing biaxial applied stress for particular creep temperature (i.e. 1210 K). In the secondary stage of creep (R2), as expected, effective creep rate is found to be almost constant. It can be seen from Fig. 3 that creep rate is increased in the tertiary stage of creep (R3) for 1.4 GPa, 2 GPa, 2.5 GPa, and 3 GPa applied stress. Effective creep rate in the tertiary stage of creep is found to be increased with increasing applied stress. Creep rate curve in the tertiary stage of creep is observed to be shifted towards upward with increasing biaxial applied stress.

Calculation of stress exponent during biaxial creep process

Minimum creep rate verse applied stress (σ) for NC Ni at 1210 K temperature is represented in Fig. 4(a). It is observed

Fig. 2 Biaxial effective creep-time curves of NC Ni for five different stresses at 1210 K temperature. (R1 → Primary stage of creep, R2 → Secondary stage of creep, and R3 → Tertiary stage of creep)



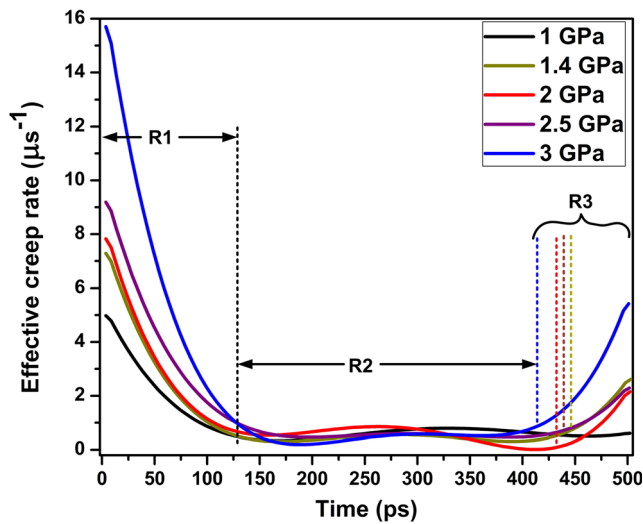


Fig. 3 Biaxial effective creep rate-time curves of NC Ni for five different stresses at 1210 K temperature. (R1 → Primary stage of creep, R2 → Secondary stage of creep, and R3 → Tertiary stage of creep)

that the minimum creep rate is increased linearly with increasing applied stress. Plot of logarithmic of minimum creep rate vs. logarithmic applied stress for NC Ni is represented in Fig. 4(b) to determine the stress exponent (*m*) under biaxial creep process. Biaxial creep characteristics for minimum (or steady state) creep rate can be explained by the Norton’s power law expression [18].

$$\dot{\epsilon}_{\min} = A\sigma^m \tag{15}$$

where $\dot{\epsilon}_{\min}$ is the minimum creep rate, σ is an external stress, *m* is a stress exponent, and *A* is a constant. The analysis of stress exponent for NC Ni using Eq. (15) is shown in Fig. 4(b). At 1210 K, *m* = 1.30, may imply that the diffusion control creep mechanism is operative [74, 75]. However, only on the basis of stress exponent analysis, it is impossible to identify an exact creep mechanism.

Atomic structure analysis during biaxial creep deformation process

Atomic configuration snapshots of NC Ni during biaxial creep process for different creep time period such as 0 ps, 100 ps, 200 ps, 300 ps, 400 ps, and 500 ps at 1210 K and 3 GPa stresses are represented in Fig. 5 and colour code of atomic snapshots is taken according to centrosymmetry parameter (CSP) (colour code range value is taken from 0 to 6 for better visualization). It can be seen that microstructure of ultra-fine grained NC Ni is almost unchanged in the primary stage of creep. But grain boundary (GB) diffusion is observed in the primary stage of creep (refer Fig. 5(b)). After the primary stage of creep, GB diffusion (called Coble creep [76]) as well as grain boundary sliding (called Lifshitz sliding [77]) mechanisms for NC Ni are observed in the secondary and tertiary stage of creep (refer Fig. 5(c–f)). The underlying GB diffusion and grain boundary sliding mechanisms, which are responsible for the deformation of NC Ni under biaxial creep process, are observed. It indicates that the diffusion-mediated creep deformation mechanism is active during biaxial creep process. Figure 5 shows that the lattice diffusion mechanism is slightly initiated during biaxial creep deformation process at 3 GPa applied stress. During biaxial creep deformation process, it can be seen that GB diffusion and grain boundary sliding mechanism may assist the grain growth. Stress-induced grain growth for NC Ni is also observed during biaxial creep process previously by Gianola et al., which also influences deformation behaviour [78].

Dislocation analysis during biaxial creep deformation process

Figure 6 shows the dislocation density vs. time curves during biaxial creep deformation process for different applied biaxial stress. Dislocation density is found to be increased with

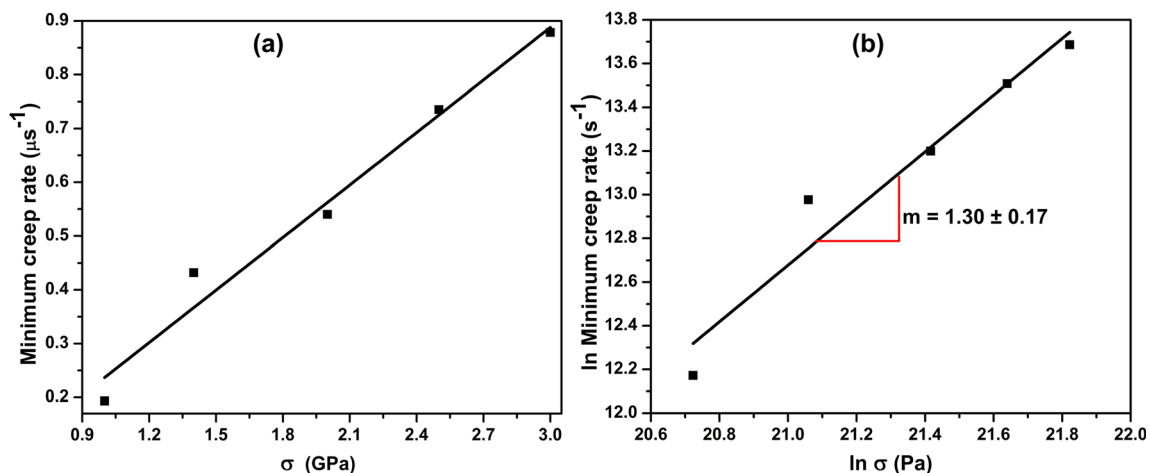


Fig. 4 Plots a minimum creep rate vs. applied stress (σ) and b logarithmic of minimum creep rate vs. logarithmic σ

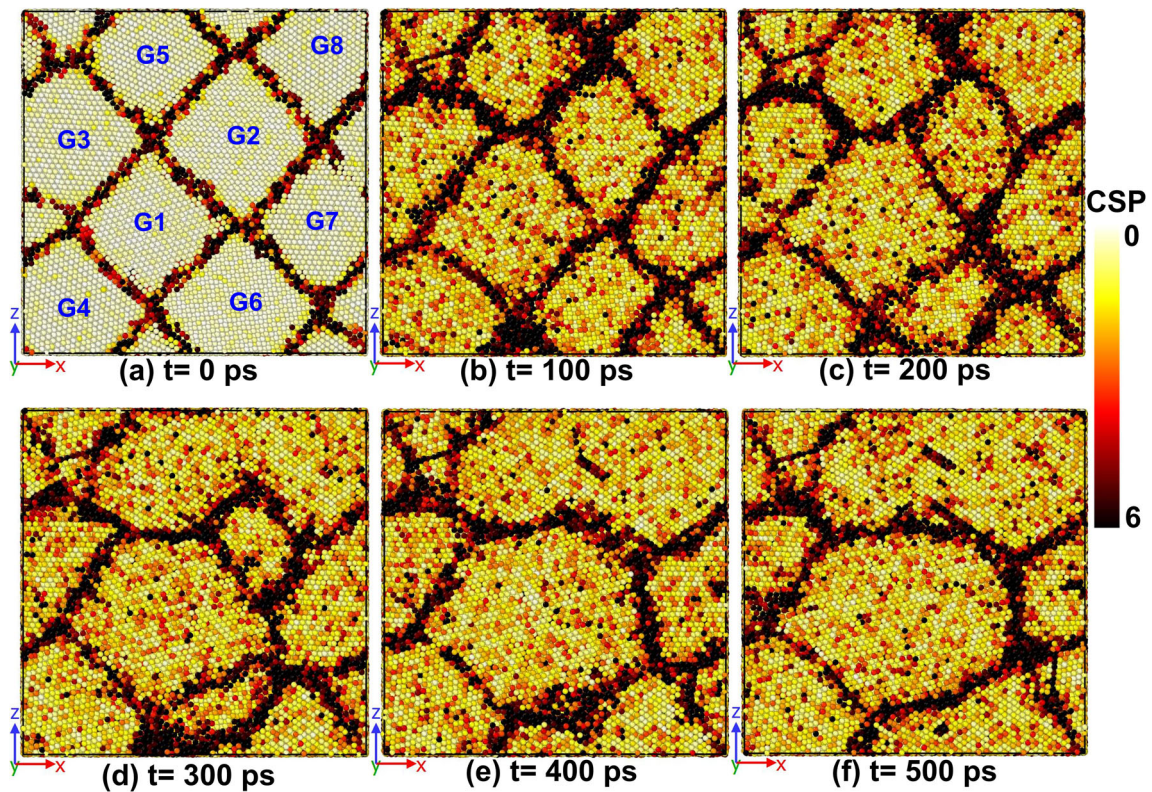
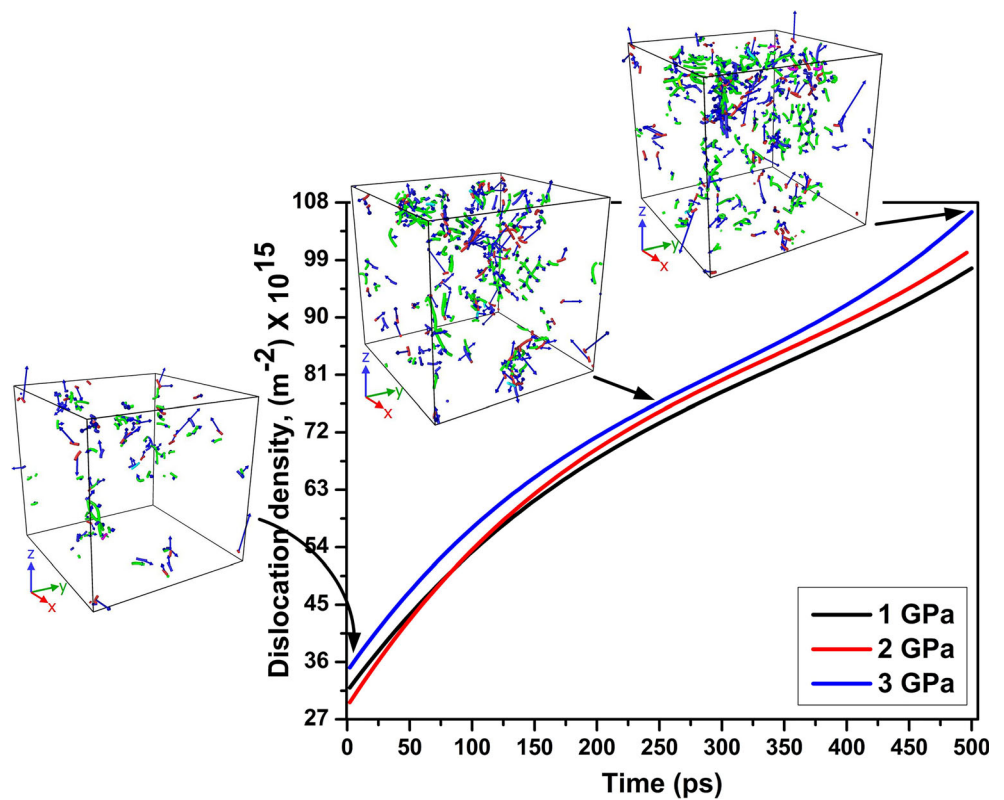


Fig. 5 Atomic snapshots (colour according to CSP) of NC Ni after different time period of creep during biaxial creep process for 3 GPa applied stress and 1210 K temperature

Fig. 6 Plots of dislocation density vs. time during biaxial creep process for different applied stress at 1210 K temperature. An inset shows dislocation snapshots at three different positions of creep time for 3 GPa applied stress



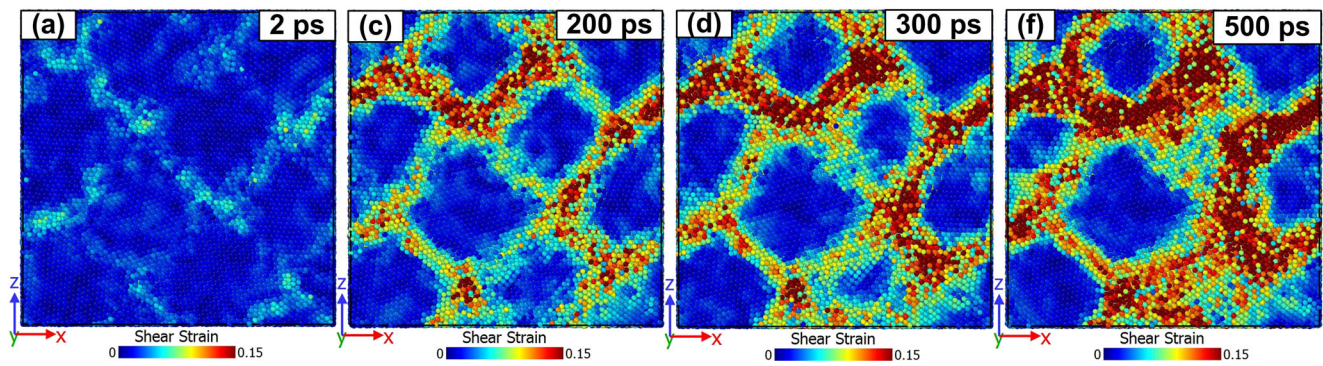


Fig. 7 Atomic snapshots of shear strains after different time period of creep during biaxial creep process for 3 GPa applied stress and 1210 K temperature

increasing creep time. It is observed that with increasing applied stress, dislocation density is shifted upward for NC Ni. It indicates the dislocation nucleation, formation and movement in NC Ni are increased with the increase of applied stress during biaxial creep deformation. It can be seen from Figs. 6 and 2 that the behaviour of dislocation density curves supports the nature of biaxial creep curves. Representative snapshots of dislocation, which is contained in the specimen (shown as inset in Fig. 6), are shown after 2 ps, 250 ps and 500 ps creep time period at 3 GPa applied stress. Different types of dislocations such as Shockley partial (green colour), Stair-rod (pink colour), Hirth partial (yellow colour), perfect dislocation (blue colour) and Frank partial (cyan colour) with Burger vector (blue colour with arrowhead) are shown inside the simulation cell. It is evident from Fig. 6 that dislocation is also assisted to deform of NC Ni materials during biaxial creep process and it

is indicated by simulation that dislocation-mediated creep deformation mechanism is also operative [79, 80].

Atomic strain and atomic trajectory analysis during biaxial creep deformation process

Atomic snapshots of shear strain after 2 ps, 200 ps, 300 ps and 500 ps time period of creep at 3 GPa applied stress during biaxial creep process is represented in Fig. 7. It is observed that higher shear strains accumulation occurs at grain boundary region with the progress of biaxial creep deformation. Figure 8 shows the atomic displacement vector trajectory snapshots for NC Ni after 2 ps, 100 ps, 300 ps and 500 ps time period of creep at 1210 K creep temperature and 3 GPa applied stress. It is found that the movement of the atoms mainly occurs at grain boundary region during creep

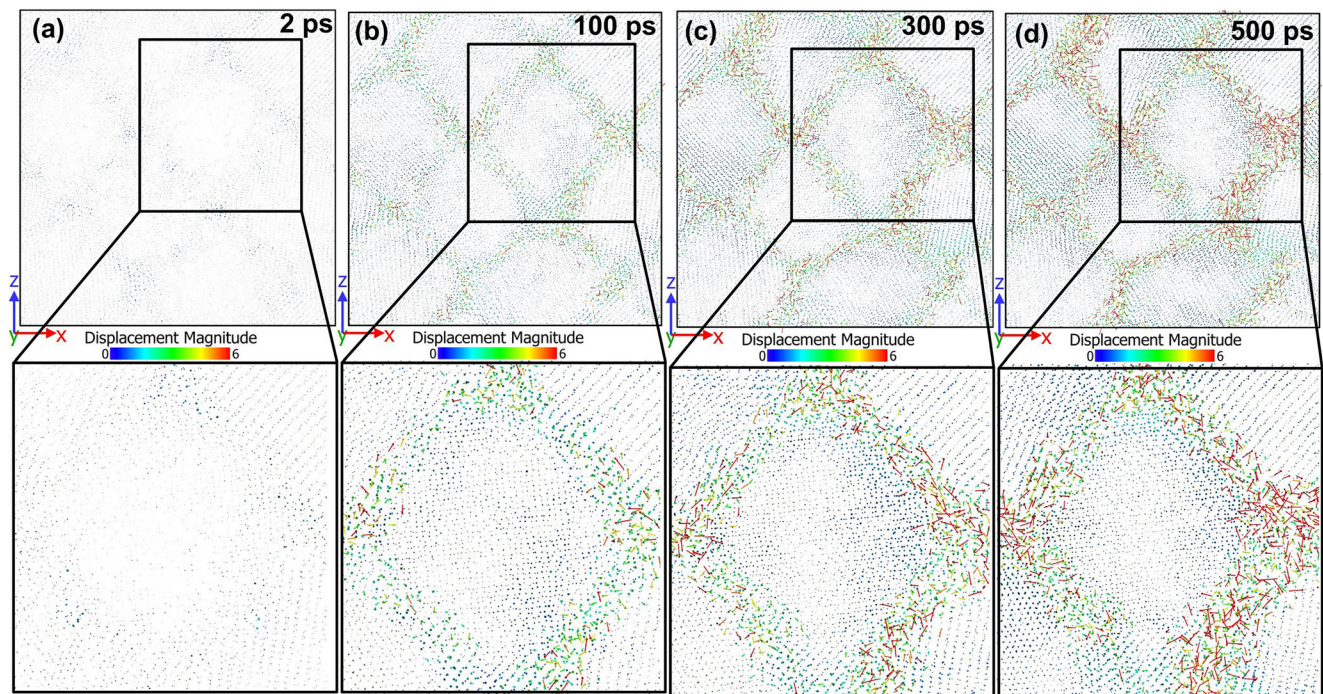


Fig. 8 Atomic displacement vector snapshots after different time period of creep during biaxial creep process for 3 GPa applied stress and 1210 K temperature

deformation. The trajectory of atoms indicates that atomic diffusion is more intensified in grain boundary regions during biaxial creep deformation of ultrafine grained NC Ni. At this juncture, it can be inferred that grain boundary diffusion as well as dislocation controlled deformation both mechanisms are operative during biaxial creep deformation process ultrafine-grained NC Ni (refer Figs. 5, 6, 7, and 8).

Grain structure evolution during biaxial creep deformation process

Overall grain structure evolution during biaxial creep deformation is investigated using grain tracking algorithm (GTA) and it is represented in Figs. 9, 10, and 11. The stress dependence on grain rotation during biaxial creep deformation process is analysed in this study using the GTA. The grain rotation during creep process for all grains as a function of creep time for

different applied stresses (i.e. 1 GPa, 2 GPa and 3 GPa) is represented in Fig. 9. The grain rotation for NC Ni has been measured in terms of the orientation after different creep deformation times with respect to the original orientation just before the creep process. It is observed from Fig. 9 that with increasing creep deformation process as a function of time, grain rotation for almost all grains is significantly increased for almost all cases of applied stresses (i.e. 1 GPa, 2 GPa and 3 GPa). Similar pattern of average grain rotation with respect to the number of cycle for NC material is reported in literature under cyclic deformation condition [41]. On the other hand, grain rotation curves for some specific grains such as G2, G5, G6, G12, G13 and G14 are found to be shifted downward with increasing applied stress during biaxial creep deformation process (refer Fig. 9). It is also found that the rotation magnitude of the G1, G3, G8, and G13 grains are found to be increased up to certain creep time and then decreased with the progress of

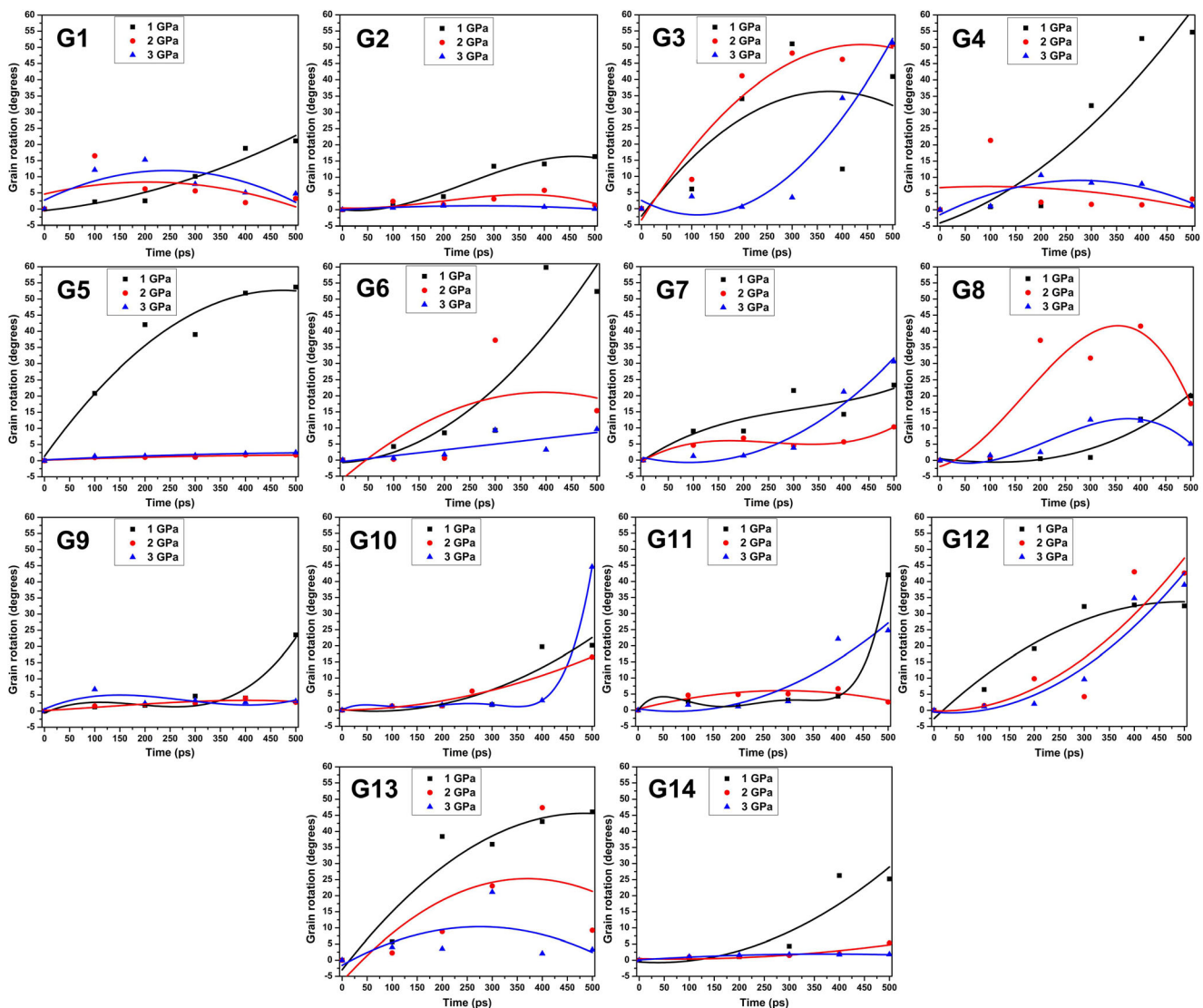


Fig. 9 Plots of grain rotation vs. time during biaxial creep process for each grain at **a** 1 GPa, **b** 2 GPa and **c** 3 GPa applied stress and 1210 K temperature

Fig. 10 Inverse pole stereographic projections for a 1 GPa, b 2 GPa and c 3 GPa applied stress at 1210 K temperature to show the evolution of the orientations and distribution of random texture for all grains during biaxial creep process

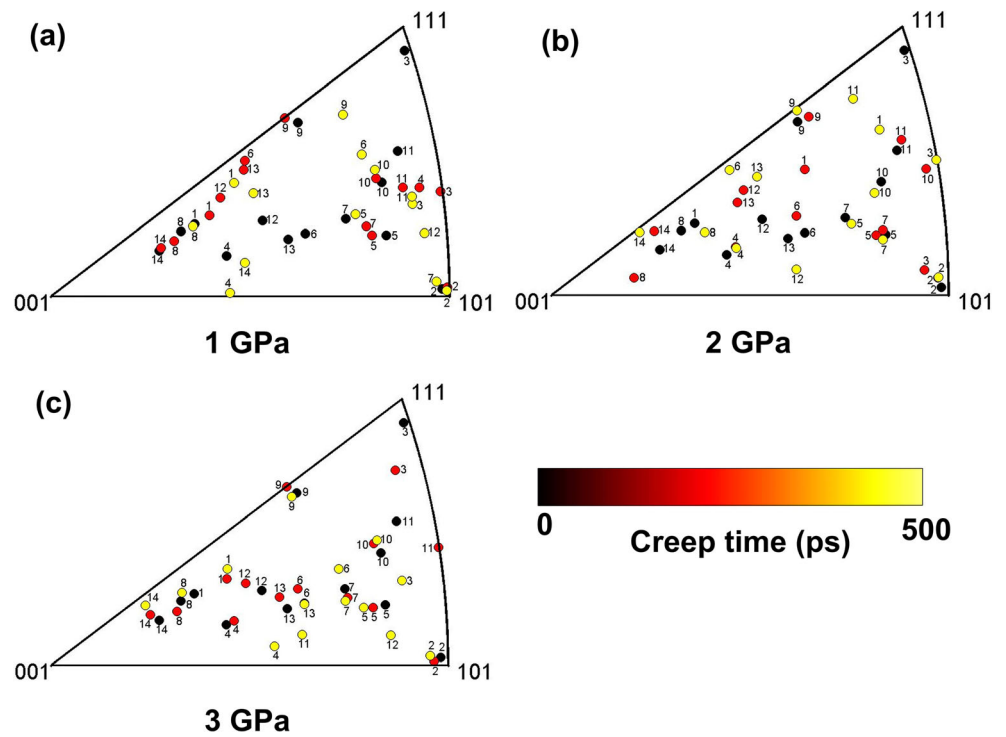
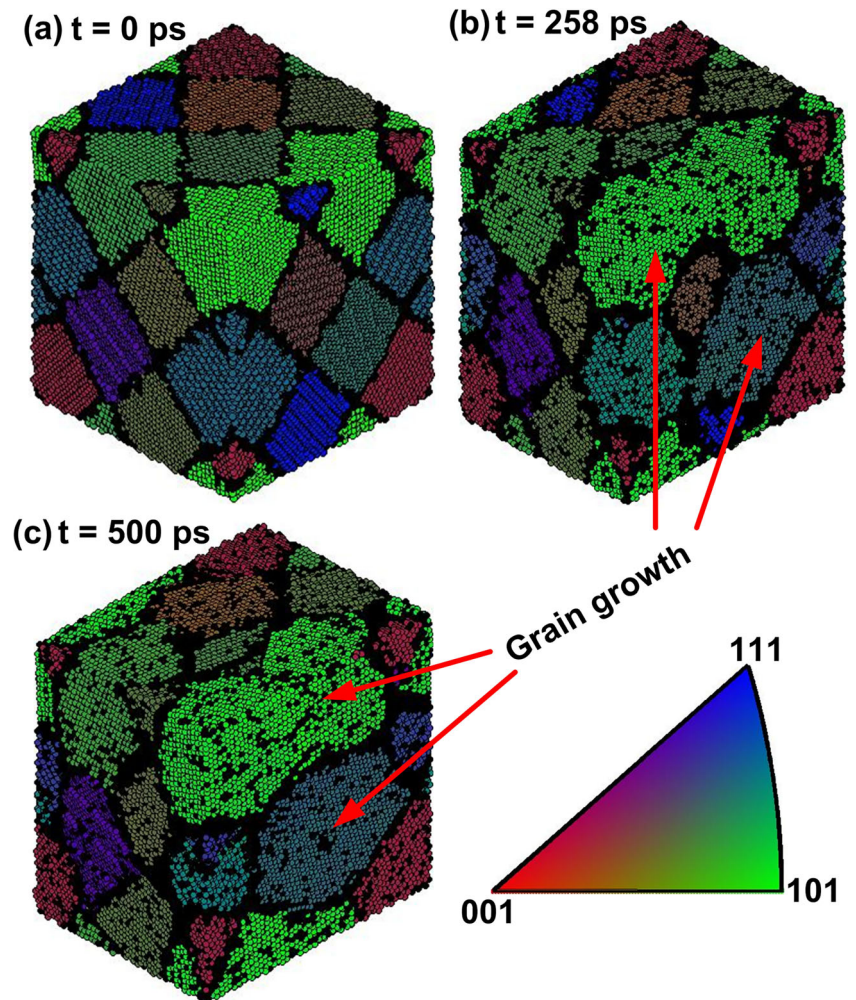


Fig. 11 Orientation map snapshots of the random NC Ni after a 0 ps, b 258 ps and c 500 ps of creep time at 3 GPa applied stress and 1210 K temperature, showing the distribution random texture for all grain during biaxial creep process



creep deformation (refer Fig. 9). It can be seen from Fig. 9 that multiple numbers of grains are experienced much larger grain rotation during biaxial creep deformation.

The inverse pole figures during biaxial creep process, having grains are labelled on the basis of the creep deformation time, are represented in Fig. 10. The inverse pole figures are assisted to visualize specific types of textures. It gives the information related to the orientation of grains in the specimen with respect to reference of crystallographic directions. The inverse pole figures plots are clearly demonstrated effective grain rotation in the specimen at different applied biaxial load. During biaxial creep deformation process, all the grains contained in the specimen are tracked as a function of creep time for three different applied stresses and subsequently analysed. It can be seen that grain rotation is occurred during biaxial creep deformation process and exhibits almost distinct distribution (refer Fig. 10). It is found that all the grain rotations are clearly visualized in inverse pole figures (texture map) by displacement of each point of grains during creep deformation process at all applied stresses. It is indicated that the inverse pole figures are influenced by applied stress. Stress-induced grain rotation happens during creep process. Grain rotation during deformation is assisted as a result of atomic shuffling within the grain boundaries [40, 41, 81, 82]. It can be inferred from Fig. 10 that there is slightly altered in texture evolved with the increase in applied stress during biaxial creep deformation process. Crystallographic orientation map for NC Ni specimen after 0 ps (initial sample), 258 ps and 500 ps creep time during creep deformation process (colours code according to inverse poles for number of grains) are represented in Fig. 11. Orientation map distribution for all grains of NC Ni is parallel to the simulation Z [0 0 1] direction. Small triangular colour code, which is shown in Fig. 11 (below lower side), is used to identify the crystallographic orientation of each grain. In this study, atomic snapshots for NC Ni during biaxial creep process are analysed by GTA. Grain growth, small grain disappearance and grain boundary migration during creep deformation process are observed to be occurred simultaneously with increasing creep time (refer Fig. 11) and it is analysed using GTA. Grain growth is a common type of the structural evolution for NC materials and is reported in literature during deformation [41, 78, 83]. However, the changes of crystallographic orientation for NC Ni during biaxial creep process are achieved using GTA to extract final structure of texture.

Conclusions

In summary, molecular dynamics (MD) simulation is used for the first time to identify the biaxial creep behaviour of NC Ni for various applied stress at 1210 K temperature. Structural evaluation as well as underlying deformation mechanism is

also investigated during biaxial creep process. Overall, significant findings related to biaxial creep deformation of ultrafine NC Ni are summarized below.

1. Duration of primary creep stage and rise in effective strain are observed to be increased with the increasing applied biaxial stress.
2. It is observed that comparatively longer period of secondary creep stage occurs during biaxial creep process for ultrafine grained NC Ni as compared with the primary and tertiary stages of creep.
3. Tertiary creep regime of ultrafine grained NC Ni is absent up until 500 ps time period for the simulated biaxial creep test performed under 1 GPa constant load. Only in case of higher biaxial load, the tertiary stage of creep is observed within 500 ps creep duration.
4. During biaxial creep deformation process of ultrafine grained NC Ni, grain boundary diffusion, grain sliding and dislocation governed deformation mechanisms are found to be operative.
5. Grain rotation in ultrafine-grained NC Ni specimen is observed during biaxial creep deformation and exhibits almost distinct distribution. It is happened due to the atomic shuffling within the GBs. It is found that there is slightly changed in texture evolved with the increase in applied stress during biaxial creep deformation.
6. Stress-induced grain growth for ultrafine-grained NC Ni occurs during biaxial creep deformation process and it assists due to the GB diffusion and GB sliding mechanism.

In one sentence, the scientific contribution of the work is to provide detail underlying physics of biaxial creep deformation behaviour of NC metals, which will help to determine the strategy for widening application domain of NC metals with respect to range of service temperature, stress, and most importantly state of stress.

References

1. Murty BS, Shankar P, Raj B, Rath BB, Murdayet J (2013) Textbook of nanoscience and nanotechnology. Springer Science & Business Media, Hyderabad
2. Kelsall R, Hamley IW, Geoghegan M (2005) Nanoscale science and technology. Wiley, Chichester
3. Yue Y, Liu P, Deng Q, Ma E, Zhang Z, Han X (2012) Quantitative evidence of crossover toward partial dislocation mediated plasticity in copper single crystalline nanowires. *Nano Lett* 12(8):4045–4049
4. Yong-Hai Y, Li-Hua W, Ze Z, Xiao-Dong H (2012) Cross-over of the plasticity mechanism in nanocrystalline Cu. *Chin Phys Lett* 29(6):066201
5. Wang L, Zhang Z, Han X (2013) In situ experimental mechanics of nanomaterials at the atomic scale. *NPG Asia Mater* 5(2):1–11

6. Kang W, Merrill M, Wheeler JM (2017) In situ thermomechanical testing methods for micro/nano-scale materials. *Nanoscale* 9(8):2666–2688
7. Pal S, Meraj M, Deng C (2017) Effect of Zr addition on creep properties of ultra-fine grained nanocrystalline Ni studied by molecular dynamics simulations. *Comput Mater Sci* 126:382–392
8. Chokshi AH (2003) Diffusion, diffusion creep and grain growth characteristics of nanocrystalline and fine-grained monoclinic, tetragonal and cubic zirconia. *Scr Mater* 48(6):791–796
9. Choi IC, Kim YJ, Seok MY, Yoo BG, Kim JY, Wang Y, Jang JI (2013) Nanoscale room temperature creep of nanocrystalline nickel pillars at low stresses. *Int J Plast* 41:53–64
10. Karanjaokar N, Stump F, Geubelle P, Chasiotis I (2013) A thermally activated model for room temperature creep in nanocrystalline Au films at intermediate stresses. *Scr Mater* 68(8):551–554
11. Li J, Zhang JY, Zhang P, Wu K, Liu G, Sun J (2016) Grain size effects on microstructural stability and creep behaviour of nanotwinned Ni free-standing foils at room temperature. *Philos Mag* 96(29):3016–3040
12. Darling KA, Rajagopalan M, Komarasamy M, Bhatia MA, Hornbuckle BC, Mishra RS, Solanki KN (2016) Extreme creep resistance in a microstructurally stable nanocrystalline alloy. *Nature* 537(7620):378–381
13. Karanjaokar N, Chasiotis I (2016) Creep behavior of nanocrystalline Au films as a function of temperature. *J Mater Sci* 51(8):3701–3714
14. Tian L (2017) A short review on mechanical behavior of nanocrystalline materials. *Int J Metall Met Phys* 2(1):1–13
15. Mo K, Lv W, Tung HM, Yun D, Miao Y, Lan KC, Stubbins JF (2016) Biaxial thermal creep of alloy 617 and alloy 230 for VHTR applications. *J Eng Mater Technol* 138(3):031015
16. Sakane M, Tokura H (2002) Experimental study of biaxial creep damage for type 304 stainless steel. *Int J Damage Mech* 11(3):247–262
17. Kobayashi H, Ohki R, Itoh T, Sakane M (2017) Multiaxial creep damage and lifetime evaluation under biaxial and triaxial stresses for type 304 stainless steel. *Eng Fract Mech* 174:30–43
18. Tung HM, Mo K, Stubbins JF (2014) Biaxial thermal creep of Inconel 617 and Haynes 230 at 850 and 950°C. *J Nucl Mater* 447(1–3):28–37
19. Mathew MD, Ravi S, Vijayanand VD, Latha S, Dasgupta A, Laha K (2014) Biaxial creep deformation behavior of Fe–14Cr–15Ni–Ti modified austenitic stainless steel fuel cladding tube for sodium cooled fast reactor. *Nucl Eng Des* 275:17–22
20. Kurtz RJ, Hamilton ML (2000) Biaxial thermal creep of V–4Cr–4Ti at 700 C and 800 C. *J Nucl Mater* 283:628–632
21. Li Y, Li S, Huang M, Li Z (2015) Analytical solution for Coble creep in polycrystalline materials under biaxial loading. *Mech Mater* 91(1):290–294
22. Peter D, Pfetzinger J, Wagner MX, Eggeler G (2009) Microstructural anisotropy, uniaxial and biaxial creep behavior of Ti–45Al–5Nb–0.2 B–0.2 C. *Mater Sci Eng A* 510:368–372
23. Li M, Nagasaka T, Hoelzer DT, Grossbeck ML, Zinkle SJ, Muroga T, Fukumoto K, Matsui H, Narui M (2007) Biaxial thermal creep of two heats of V4Cr4Ti at 700 and 800 C in a liquid lithium environment. *J Nucl Mater* 367:788–793
24. Hyde TH, Sun W (2006) Creep failure behaviour of a 9CrMoNbV weld metal with anisotropy under a biaxial loading state. *J Strain Anal Eng Des* 41(5):369–380
25. Murty KL, Tanikella BV, Earthman JC (1994) Effect of grain shape and texture on equi-biaxial creep of stress relieved and recrystallized zircaloy-4. *Acta Metall Mater* 42(11):3653–3661
26. Murthy KL (1992) Biaxial creep behavior of textured zircaloy tubing. *JOM* 44(2):49–55
27. Trivaudey F, Delobelle P (1990) High temperature creep damage under biaxial loading—part I: experiments. *J Eng Mater Technol* 112(4):442–449
28. Murty KL, Adams BL (1985) Biaxial creep of textured zircaloy I: experimental and phenomenological descriptions. *Mater Sci Eng* 70:169–180
29. Kumar KS, Swygenhoven HV, Suresh S (2003) Mechanical behavior of nanocrystalline metals and alloys. *Acta Mater* 51(19):5743–5774
30. Meyers MA, Mishra A, Benson DJ (2006) Mechanical properties of nanocrystalline materials. *Prog Mater Sci* 51(4):427–556
31. Schiotz J, Di Tolla FD, Jacobsen KW (1998) Softening of nanocrystalline metals at very small grain sizes. *Nature* 391(6667):561–563
32. Schiotz J, Vegge T, Di Tolla FD, Jacobsen KW (1999) Atomic-scale simulations of the mechanical deformation of nanocrystalline metals. *Phys Rev B* 60(17):11971
33. Swygenhoven HV, Derlet PM (2001) Grain-boundary sliding in nanocrystalline fcc metals. *Phys Rev B* 64(22):224105
34. Ke M, Hackney SA, Milligan WW, Aifantis EC (1995) Observation and measurement of grain rotation and plastic strain in nanostructured metal thin films. *Nanostruct Mater* 5(6):689–697
35. Shan Z, Stach EA, Wiezorek JMK, Knapp JA, Follstaedt DM, Mao SX (2004) Grain boundary-mediated plasticity in nanocrystalline nickel. *Science* 305(5684):654–657
36. Farkas D, Mohanty S, Monk J (2007) Linear grain growth kinetics and rotation in nanocrystalline Ni. *Phys Rev Lett* 98(16):165502
37. Cahn JW, Taylor JE (2004) A unified approach to motion of grain boundaries, relative tangential translation along grain boundaries, and grain rotation. *Acta Mater* 52(16):4887–4898
38. Legros M, Gianola DS, Hemker KJ (2008) In situ TEM observations of fast grain-boundary motion in stressed nanocrystalline aluminum films. *Acta Mater* 56(14):3380–3393
39. Rupert TJ, Gianola DS, Gan Y, Hemker KJ (2009) Experimental observations of stress-driven grain boundary migration. *Science* 326(5960):1686–1690
40. Upmanyu M, Srolovitz DJ, Lobkovsky AE, Warren JA, Carter WC (2006) Simultaneous grain boundary migration and grain rotation. *Acta Mater* 54(7):1707–1719
41. Panzarino JF, Ramos JJ, Rupert TJ (2015) Quantitative tracking of grain structure evolution in a nanocrystalline metal during cyclic loading. *Model Simul Mater Sci Eng* 23(2):025005
42. Hasnaoui A, Swygenhoven HV, Derlet PM (2002) Cooperative processes during plastic deformation in nanocrystalline fcc metals: a molecular dynamics simulation. *Phys Rev B* 66(18):184112
43. Rupert TJ (2013) Strain localization in a nanocrystalline metal: atomic mechanisms and the effect of testing conditions. *J Appl Phys* 114(3):033527
44. Haque MA, Saif MTA (2005) In situ tensile testing of nanoscale freestanding thin films inside a transmission electron microscope. *J Mater Res* 20(7):1769–1777
45. Zheng K, Han X, Wang L, Zhang Y, Yue Y, Qin Y, Zhang X, Zhang Z (2009) Atomic mechanisms governing the elastic limit and the incipient plasticity of bending Si nanowires. *Nano Lett* 9(6):2471–2476
46. Yue Y, Liu P, Zhang Z, Han X, Ma E (2011) Approaching the theoretical elastic strain limit in copper nanowires. *Nano Lett* 11(8):3151–3155
47. Wang L, Lu Y, Kong D, Xiao L, Sha X, Sun J, Zhang Z, Han X (2015) Dynamic and atomic-scale understanding of the twin thickness effect on dislocation nucleation and propagation activities by in situ bending of Ni nanowires. *Acta Mater* 90:194–203
48. Han X, Wang L, Yue Y, Zhang Z (2015) In situ atomic scale mechanical microscopy discovering the atomistic mechanisms of plasticity in nano-single crystals and grain rotation in polycrystalline metals. *Ultramicroscopy* 151:94–100

49. Wang J, Zeng Z, Weinberger CR, Zhang Z, Zhu T, Mao SX (2015) In situ atomic-scale observation of twinning-dominated deformation in nanoscale body-centred cubic tungsten. *Nat Mater* 14(6):594
50. Wang L, Teng J, Sha X, Zou J, Zhang Z, Han X (2017) Plastic deformation through dislocation saturation in ultrasmall Pt nanocrystals and its in situ atomistic mechanisms. *Nano Lett* 17(8):4733–4739
51. Bhatia MA, Mathaudhu SN, Solanki KN (2015) Atomic-scale investigation of creep behavior in nanocrystalline Mg and Mg–Y alloys. *Acta Mater* 99:382–391
52. Pal S, Meraj M (2016) Structural evaluation and deformation features of interface of joint between nano-crystalline Fe–Ni–Cr alloy and nano-crystalline Ni during creep process. *Mater Des* 108:168–182
53. Meraj M, Pal S (2016) The effect of temperature on creep behaviour of porous (1 at.%) nano crystalline nickel. *Trans Indian Inst Metals* 69(2):277–282
54. Meraj M, Yedla N, Pal S (2016) The effect of porosity and void on creep behavior of ultra-fine grained nano crystalline nickel. *Mater Lett* 169:265–268
55. Nie K, Wu WP, Zhang XL, Yang SM (2017) Molecular dynamics study on the grain size, temperature, and stress dependence of creep behavior in nanocrystalline nickel. *J Mater Sci* 52(4):2180–2191
56. Meraj M, Pal S (2017) Healing mechanism of nanocrack in nanocrystalline metals during creep process. *Appl Phys A Mater Sci Process* 123(2):138
57. Meraj M, Pal S (2017) Nano-scale simulation based study of creep behavior of bimodal nanocrystalline face centered cubic metal. *J Mol Model* 23(11):309
58. Meraj M, Pal S (2017) Comparative creep behaviour study between single crystal nickel and ultra-fine grained nano crystalline nickel in presence of porosity at 1120 K temperature. *Metall Res Technol* 114(1):107
59. Meraj M, Pal S (2017) Effect of temperature and stress on creep behavior of ultrafine grained nanocrystalline Ni-3 at% Zr alloy. *Met Mater Int* 23(2):272–282
60. Pal S, Mishra S, Meraj M, Mondal AK, Ray BC (2018) On the comparison of interrupted and continuous creep behaviour of nanocrystalline copper: a molecular dynamics approach. *Mater Lett* 229:256–260
61. Saha S, Motalab M (2018) Nature of creep deformation in nanocrystalline tungsten. *Comput Mater Sci* 149:360–372
62. Yamakov V, Wolf D, Phillpot SR, Gleiter H (2002) Grain-boundary diffusion creep in nanocrystalline palladium by molecular-dynamics simulation. *Acta Mater* 50(1):61–73
63. Millett PC, Desai T, Yamakov V, Wolf D (2008) Atomistic simulations of diffusional creep in a nanocrystalline body-centered cubic material. *Acta Mater* 56(14):3688–3698
64. Wang YJ, Ishii A, Ogata S (2011) Transition of creep mechanism in nanocrystalline metals. *Phys Rev B* 84(22):224102
65. Wang YJ, Ishii A, Ogata S (2013) Entropic effect on creep in nanocrystalline metals. *Acta Mater* 61(10):3866–3871
66. Chen D (1995) Structural modeling of nanocrystalline materials. *Comput Mater Sci* 3(3):327–333
67. Nose S (1984) A unified formulation of the constant temperature molecular dynamics methods. *J Chem Phys* 81(1):511–519
68. Hoover WG (1985) Canonical dynamics: equilibrium phase-space distributions. *Phys Rev A* 31(3):1695
69. Berendsen HJ, Postma JV, van Gunsteren WF, DiNola ARHJ, Haak JR (1984) Molecular dynamics with coupling to an external bath. *J Chem Phys* 81(8):3684–3690
70. Plimpton S (1995) Fast parallel algorithms for short-range molecular dynamics. *J Comput Phys* 117(1):1–19
71. Mendelev MI, Kramer MJ, Hao SG, Ho KM, Wang CZ (2012) Development of interatomic potentials appropriate for simulation of liquid and glass properties of NiZr2 alloy. *Philos Mag* 92(35):4454–4469
72. Stukowski A (2009) Visualization and analysis of atomistic simulation data with OVITO—the open visualization tool. *Model Simul Mater Sci Eng* 18(1):015012
73. Panzarino JF, Rupert TJ (2014) Tracking microstructure of crystalline materials: a post-processing algorithm for atomistic simulations. *JOM* 66(3):417–428
74. Wang N, Wang Z, Aust KT, Erb U (1997) Room temperature creep behavior of nanocrystalline nickel produced by an electrodeposition technique. *Mater Sci Eng A* 237(2):150–158
75. Luthy H, White RA, Sherby OD (1979) Grain boundary sliding and deformation mechanism maps. *Mater Sci Eng* 39(2):211–216
76. Coble RL (1963) A model for boundary diffusion controlled creep in polycrystalline materials. *J Appl Phys* 34(6):1679–1682
77. Lifshitz IM (1963) On the theory of diffusion-viscous flow of polycrystalline bodies. *Soviet Physics JETP* 17(4):909
78. Gianola DS, Van Petegem S, Legros M, Brandstetter S, Van Swygenhoven H, Hemker KJ (2006) Stress-assisted discontinuous grain growth and its effect on the deformation behavior of nanocrystalline aluminum thin films. *Acta Mater* 54(8):2253–2263
79. Kassner ME, Smith KK, Campbell CS (2015) Low-temperature creep in pure metals and alloys. *J Mater Sci* 50(20):6539–6551
80. Reddy KV, Pal S (2018) Influence of dislocations, twins, and stacking faults on the fracture behavior of nanocrystalline Ni nanowire under constant bending load: a molecular dynamics study. *J Mol Model* 24(10):277
81. Gutkin MY, Ovid'ko IA, Skiba NV (2003) Crossover from grain boundary sliding to rotational deformation in nanocrystalline materials. *Acta Mater* 51(14):4059–4071
82. Ovid'ko IA, Sheinerman AG (2008) Special rotational deformation in nanocrystalline metals and ceramics. *Scr Mater* 59(1):119–122
83. Xu W, Dai P, Wu X (2010) Effect of stress-induced grain growth during room temperature tensile deformation on ductility in nanocrystalline metals. *Bull Mater Sci* 33(5):561–568

Publisher's note Springer Nature remains neutral with regard to jurisdictional claims in published maps and institutional affiliations.